JOURNAL OF GEOPHYSICAL RESEARCH, VOL. 113, F03011, doi:10.1029/2008JF001005, 2008

Seismic and hydroacoustic tremor generated by colliding icebergs

D. R. MacAyeal,[1] E. A. Okal,[2] R. C. Aster,[3] and J. N. Bassis[4]

Received 22 February 2008; revised 15 May 2008; accepted 19 June 2008; published 1 August 2008.

[1] Iceberg harmonic tremor (IHT) emanating from tabular icebergs in the Southern Ocean and along calving margins of the Antarctic Ice Sheet is a complex, evolving signal at frequencies above approximately 0.5 Hz. IHT has been observed as T phases on islands in the equatorial Pacific, as hydroacoustic signals in the Indian Ocean, and by local and regional Antarctic seismic networks. To identify the IHT source mechanism and to understand its relevance to iceberg calving, evolution, and breakup, we deployed seismometers on a giant (25 by 50 km) tabular iceberg called C16 in the Ross Sea, Antarctica, during a uniquely accessible period (austral summer, 2003–2004) when it was aground against the northern shore of Ross Island. During the deployment period, C16 was in sporadic contact with another giant tabular iceberg, B15A, that was moving under the influence of local ocean currents. This study reveals that the C16-associated IHT was a manifestation of extended episodes of discrete, repeating stick-slip icequakes (typically thousands of individual subevents per hour) produced when the cliff-like edges of the tabular icebergs underwent glancing, strike-slip collisions. The IHT signal that we observed is thus not a phenomenon associated with iceberg elastic or fluid resonance modes, but is instead the consequence of long sequences of very regularly spaced and similar pulses of seismic radiation from these constituent stick-slip subevents. IHT represents a newly identified glaciogenic source of seismicity that can be used to improve our understanding of iceberg dynamics and possibly of ice shelf disintegration processes.

Citation: MacAyeal, D. R., E. A. Okal, R. C. Aster, and J. N. Bassis (2008), Seismic and hydroacoustic tremor generated by colliding icebergs, *J. Geophys. Res.*, *113*, F03011, doi:10.1029/2008JF001005.

1. Introduction

[2] Iceberg harmonic tremor (IHT) is a recently discovered seismic and hydroacoustic signal associated with Antarctic icebergs, both adrift and aground [*Talandier et al.*, 2002, 2006]. The observational signatures of IHT are its uninterrupted duration lasting up to ~4 h, its time variable fundamental frequency in the 1 Hz to 10 Hz range, and the multiple harmonic frequencies that sometimes display as striations on spectrograms of IHT. Heretofore, IHT has been observed 10s to 1000s of km from the presumed source as T phases (hydroacoustic waves that convert to local seismic waves) on islands of the equatorial Pacific [*Talandier et al.*, 2002, 2006], as seismic phases in Antarctica [*Romero*, 2004; *Müller et al.*, 2005], and as hydroacoustic signals in the Indian Ocean [*Talandier et al.*, 2006; *Chapp et al.*, 2005]. Analogies to models of tectonic and volcanic tremor suggests three possible IHT source mechanisms: (1) frictional processes where icebergs scrape against each other or across the ocean floor, (2) movements of water through englacial conduits [*Talandier et al.*, 2002; *Romero*, 2004; *Chapp et al.*, 2005; *Müller et al.*, 2005], and (3) excitation of iceberg rift reservoir modes induced by hydrodynamic instability of ocean currents moving past openings where rifts intersect the edge of the iceberg (D. Jansen and C. Müller, Iceberg generated tremor in the vicinity of South Georgia Island, submitted to *Geophysical Journal International*, 2008).

[3] In an effort to determine the source mechanism(s), we deployed a 4 station seismographic network during the Austral summer of 2003 on iceberg C16, a giant 50 km by 25 km tabular iceberg aground in the southwest Ross Sea, Antarctica (Figure 1). This iceberg was chosen because of its close proximity to B15A, a 150 by 50 km fragment of the iceberg B15 that was previously determined to radiate IHT [*Talandier et al.*, 2002], because it was routinely being struck by B15A because of the tidal drift of B15A (C16 was aground, and thus not drifting) [*MacAyeal et al.*, 2008], and

[1]Department of Geophysical Sciences, University of Chicago, Chicago, Illinois, USA.
[2]Department of Geological Sciences, Northwestern University, Evanston, Illinois, USA.
[3]Geophysical Research Center and Department of Earth and Environmental Science, New Mexico Institute of Mining and Technology, Socorro, New Mexico, USA.
[4]Institute for Geophysics and Planetary Physics, Scripps Institution of Oceanography, University of California San Diego, La Jolla, California, USA.

0148-0227/08/2008JF001005$09.00

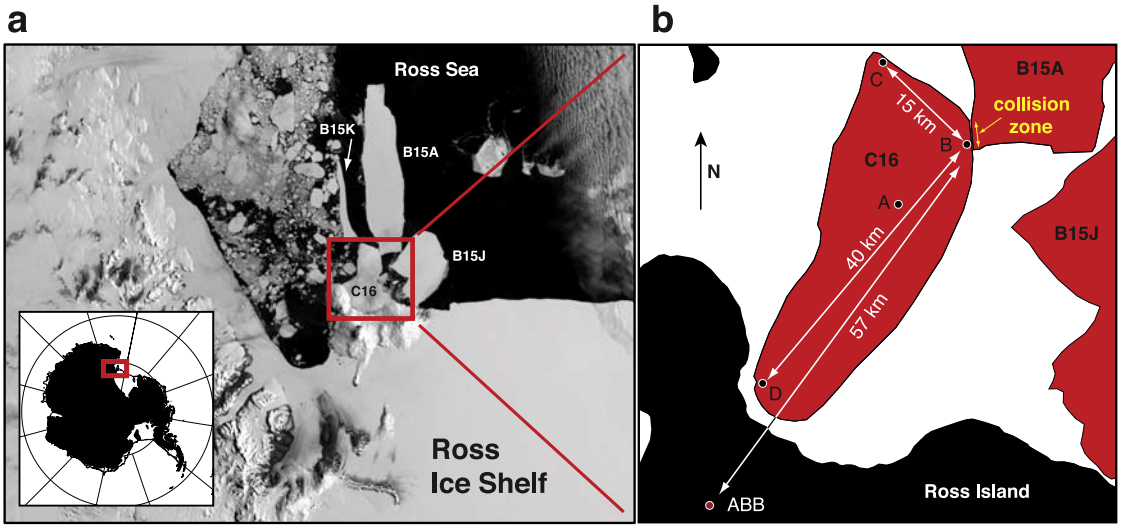

Figure 1. Seismic station locations and arrangement of icebergs. (a) Moderate Resolution Imaging Spectroradiometer (MODIS) satellite image of the southwest Ross Sea, Antarctica, at 1840 UTC on 26 December 2003 ([*Hall et al.*, 2002] see also, http://nsidc.org/data/iceshelves_images/ross_west.html). Iceberg C16 was aground and immobilized immediately north of Ross Island and the Ross Ice Shelf (see *Davey* [2004] for bathymetry). Icebergs B15A, B15J, and B15K surround C16 and are adrift. (b) Location of seismometer sites A–D at which tremor was observed during the December–January field campaign of 2003–2004. Site ABB is one of several on Ross Island maintained by the Mount Erebus Volcano Observatory [*Aster et al.*, 2004] that also recorded tremor events. The locations and shapes of the C16 and B15A boundaries are approximate and are inferred from the satellite imagery. The collision zone between B15A and C16 is the source location of all iceberg harmonic tremor (IHT) events discussed here. Colocation uncertainty between the active collision zone, determined by remote and on-site observations, and the IHT source, determined from seismogram analysis, is <1 km.

because IHT was recorded during the previous 24 months on neighboring Ross Island by seismometers of the Mount Erebus Volcano Observatory [*Aster et al.*, 2004].

2. Seismogram Analysis

2.1. IHT Spectrograms

[4] The C16 seismographic network recorded IHT almost daily between early December 2003 and mid-January 2004. Two IHT examples shown in Figure 2 are illustrative of the many examples observed, and represent episodes with (1) the strongest ground motion (27 December 2003) and (2) the most symmetric (about an aseismic "eye" illustrated in Figure 2) spectrogram pattern (19 January 2004). Vertical ground displacement spectrograms for the 19 January 2004 event (Figure 2d) shows a concave upward striated energy density signature characterized by a strong fundamental frequency component and harmonically related multiples. We refer to this signature as a "chevron" pattern, and see it in many IHT examples. In the majority of IHT spectrograms, only a single associated group of fundamental and higher harmonics are observed, suggesting a single source rather than multiple simultaneous sources. The IHT episodes begin abruptly, with a fundamental frequency above 10 Hz. As time progresses, the fundamental frequency (and its following harmonics) glides downward over a period of several hours. The signal abruptly terminates at the beginning of an aseismic eye, when the fundamental frequency has descended below ~1 Hz. The eye persists for ~5 min until the tremor signal impulsively resumes, again with a fundamental frequency beginning below ~1 Hz. The tremor lasts an additional several hours with the fundamental frequency gliding upward to above 10 Hz before terminating.

2.2. Seismic and Hydroacoustic Phase Arrivals

[5] The key observation allowing IHT source location and phases to be determined was the distinctive, abrupt "restart" signifying the start of tremor at the end of the tremor-free eye described above. The highly impulsive arrival times of the first distinct icequake subevent from the IHT restart were easily picked on each of the iceberg seismograms because these signals (1) had very high signal-to-noise, (2) identification of associated seismograms was uncomplicated by interfering phases from preceding subevents, and (3) had simple and similar waveforms across the network. Arrival times were picked graphically (the time of the leading slope of the initial wavefront was digitized visually from the graph to an accuracy of about 0.2 s, resulting in phase velocities accurate to about ±20 m s^{-1}). The distinct icequake signals signifying the posteye restart of IHT in the 27 December 2003 episode observed on the iceberg and Ross Island stations are displayed in Figure 3. To enhance clarity, Figure 3 does not plot the seismogram from iceberg station A, and plots only one Ross Island seismogram (station ABB).

[6] Arrival times for Ross Island seismograms were more difficult to obtain than for the iceberg stations, because of lower signal-to-noise levels presumably due to much greater levels of scattering and attenuation arising from the longer and more heterogeneous paths through ice, ocean, and solid

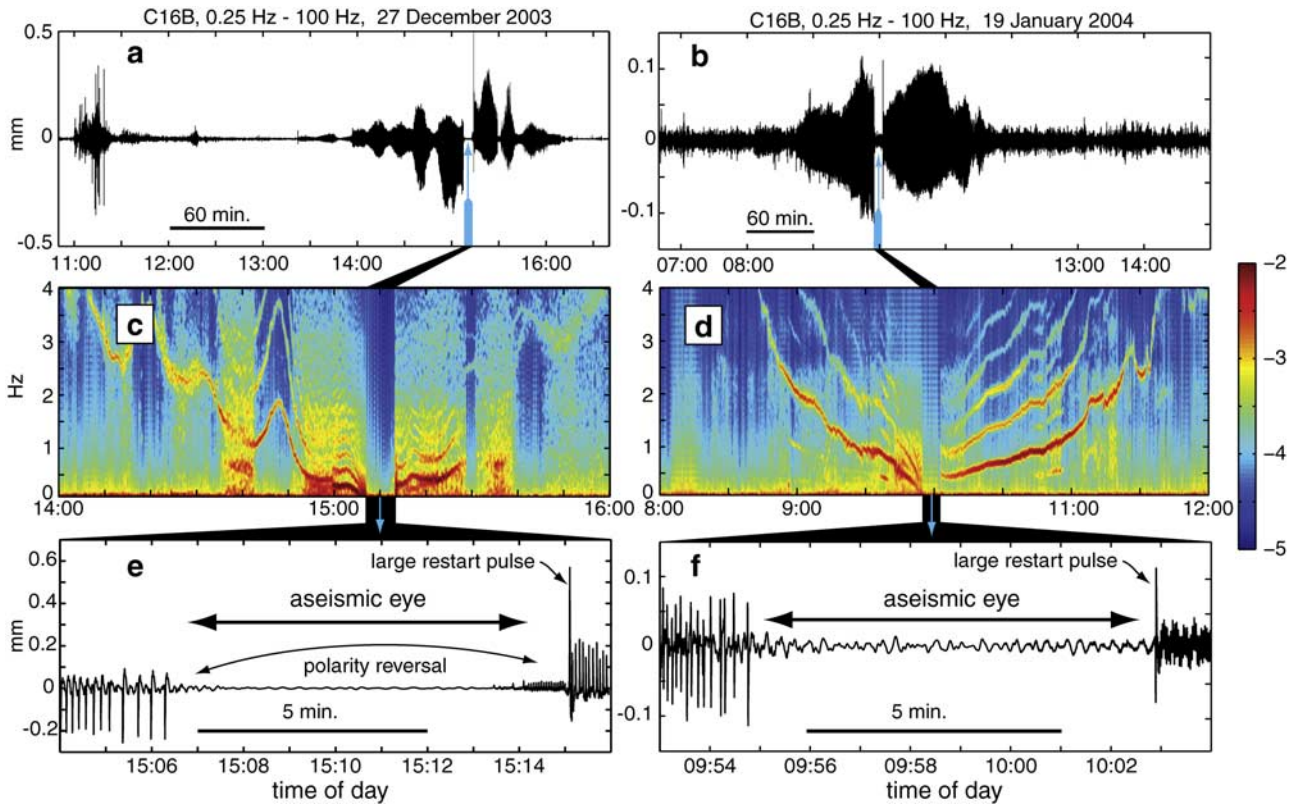

Figure 2. Two representative chevron-patterned iceberg harmonic tremor episodes recorded at iceberg C16 seismic station B (Figure 1). Source-to-receiver oriented (183°E of N azimuth) longitudinal component of ground displacement for events recorded on (a) 27 December 2003 and (b) 19 January 2004. (c and d) Spectrograms (low-pass filtered and resampled to 20 Hz using the MATLAB decimate command) of the seismograms shown in Figures 2a and 2b, respectively. IHT episodes display distinctive harmonic spectrogram character indicating a time-variable fundamental frequency with integer multiple harmonics. Color bar indicates the $\log_{10}$ of power spectral density as a function of time (horizontal axis) and frequency (vertical axis) in the spectrograms expressed in units of dB of m^2 s^2 per Hz. Spectrograms were computed using the MATLAB spectrogram command with a 600-sample Hamming window with 500-sample overlap. For clearer visual presentation, the spectrograms are smoothed by a 3 by 3 pixel averaging filter (using the MATLAB filter2 command). Aseismic eyes are seen in each pattern adjacent to where the fundamental harmonic reaches minimum frequency. (e and f) Longitudinal component of ground displacement during the aseismic eye periods highlighted in Figures 2a and 2b, respectively. Waveform polarity reverses following the aseismic eye (Figure 2e), and amplitude of the initial pulse is enhanced during tremor restart following the eye (Figures 2e and 2f). Timing of impulsive seismoacoustic phases generated at the start and end of these aseismic eyes establishes the source location. Waveform polarity reversal across the eyes, correlation between changes in the fundamental frequency and the GPS-derived velocity of B15A, and polarity of the P and S seismic radiation patterns establish the source mechanism of IHT as repeating stick-slip events at the C16/B15A collision zone (see Figure 1b).

earth. To pick the initial arrival of the restart waveform on Ross Island stations, first arrivals were estimated visually from the seismograms. Because of the complex travel paths to Ross Island stations, these data were used to constrain seismic phase velocity but were not used to determine the source location (for which the iceberg stations were used exclusively). Uncertainty of the graphical digitization technique used to determine the arrival of the first distinct icequake on the Ross Island stations was roughly 0.4 seconds, giving a phase velocity uncertainty that is roughly ±50 m s^{-1}. A second, but even more emergent, increase in the IHT envelope (i.e., above ~10 Hz) in the Ross Island seismograms occurs at a time consistent with a second, slower phase of propagation, and may represent a hydroacoustically mediated path and is a robust feature of the IHT signal observed on all the Ross Island seismograms, including those not shown in Figure 3.

[7] At least two phases of propagation are identified from filtered seismogram sections in the iceberg data, and are illustrated in Figures 3a and 3b. We refer to these two phases as "fast" and "slow," and compare their apparent phase velocity with studies of seismic propagation in ice shelves [e.g., *Kirchner and Bentley*, 1979] to identify their physical nature. At station B, which was unambiguously closest to the IHT source (determined from both phase timing and amplitude), IHT initiation clearly generated a

large-amplitude initial waveform followed by a train of discrete, repeating waveforms of smaller amplitude (i.e., as shown in the posteye tremor restart in Figures 2e and 2f). Filtering the seismograms (between 1 Hz and 3 Hz) shows that the discrete subevents in this frequency band propagate at a fast phase apparent velocity of 2925 ± 20 m s^{-1} along iceberg paths, and 4475 ± 50 m s^{-1} on Ross Island paths (Figure 3a). Filtering between 5 and 35 Hz, further reveals a distinct slow phase with an apparent velocity of 1425 ± 20 m s^{-1}, at both iceberg and Ross Island stations (Figure 3b). Effort to more systematically evaluate quantitative aspects of phase propagation velocities using the iceberg station data was not considered worthwhile because of the complexity of the iceberg thickness (largely unmeasured, but estimated to vary between ~45 m and ~150m) and density variation (i.e., that of a typical ice shelf, where density varies from ~300 to ~900 kg m^{-3}) between stations. The important result of the signal analysis shown in Figures 3a and 3b is the fact that two distinct phases, fast and slow, are seen in the iceberg and Ross Island data. This motivates our effort to interpret these distinct phases in terms of seismic and hydroacoustic behavior established in the literature for ice shelf and oceanic conditions. We interpret the fast phase observed on the iceberg as a horizontally propagating ice-transmitted P wave, consistent with velocities determined for the Ross Ice Shelf in refraction studies [*Kirchner et al.*, 1979; *Kirchner and Bentley*, 1979]. The corresponding phase observed on Ross Island is interpreted as a P wave with a short acoustic leg between the near-surface source and the ocean floor (Figure 3c). The ~4475 m s^{-1}, apparent

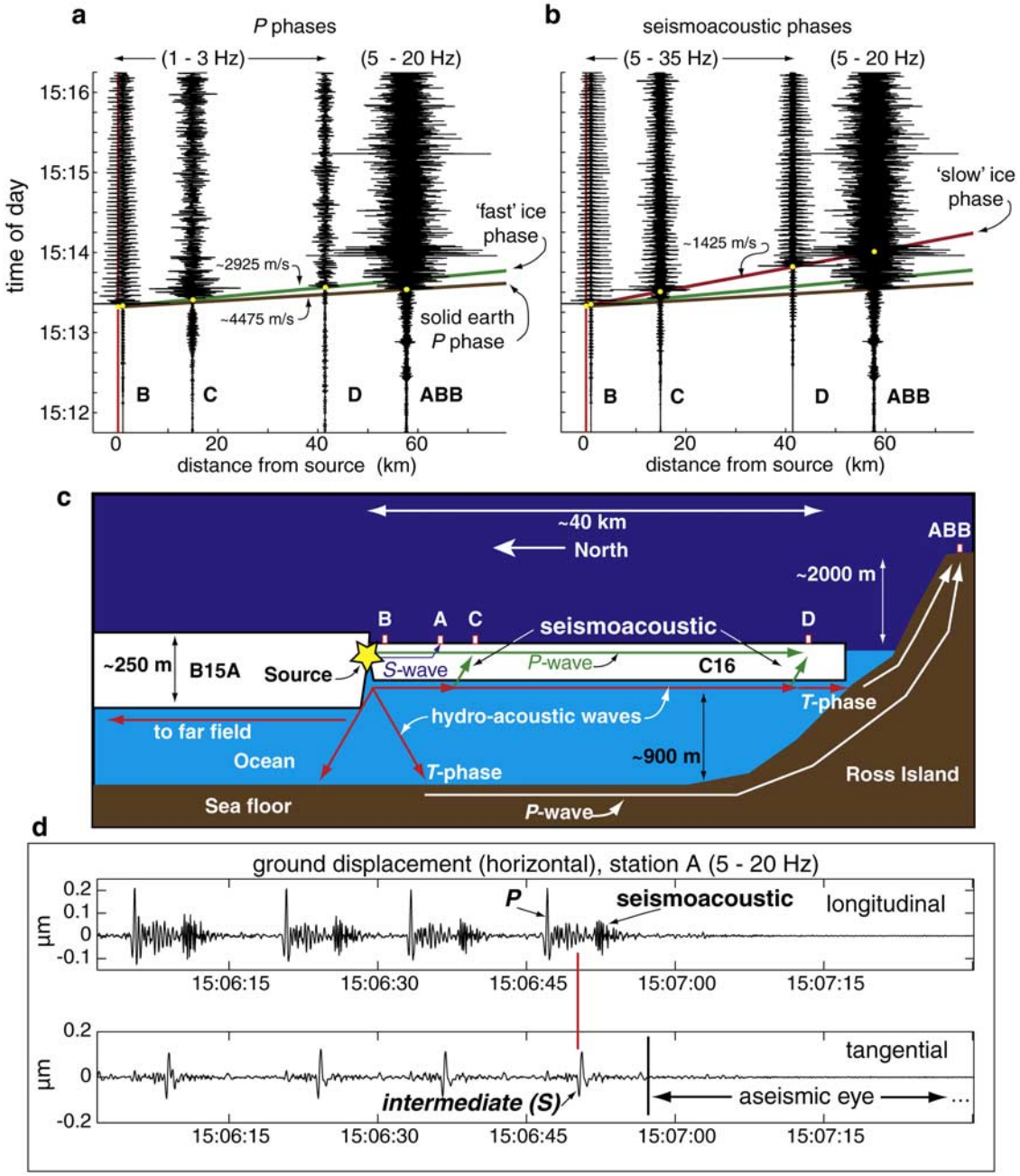

Figure 3

velocity implied by the Ross Island observations (for graphical clarity, only station ABB is shown in Figures 3a and 3b; but 4 other Ross Island stations provided similar results) necessitates the propagation path to be mostly in the solid Earth and is consistent with bulk velocity measurements of Ross Island [*Dibble et al.*, 1994]. For iceberg stations, the apparent velocity of the slow phase ($\sim$1425 m s^{-1}) is in a range of both S waves in the iceberg [*Kirchner and Bentley*, 1979] and acoustic waves in seawater [*Chen and Millero*, 1977; *Jacobs et al.*, 1985]. For the Ross Island stations, however, an S wave explanation for the slow phase (i.e., the second arrival identified by the increase in noise amplitude) is ruled out because the apparent velocity is too slow (less than the $\sim$2500 m/s expectation for S wave propagation for volcanic rocks with typical Poisson's ratio near 0.25, the ray path to ABB avoids the volcanically active region of Mount Erebus). We resolve the ambiguity for the slow iceberg phase, and explain the sub-S wave velocity propagation leading to the Ross Island stations, by noting that the slow phase is observed at all stations as a higher-frequency signal than the previously described fast P phase. At high frequency, S waves generally attenuate more strongly than P waves [*Stein and Wysession*, 2003] and would thus be expected to have lower, or at least comparable, frequency content than an associated P phase. We instead interpret the slow phase observed at both iceberg and the Ross Island stations as indicative of low-loss hydroacoustic propagation largely in the seawater below the iceberg (with appropriate conversion to P wave seismic energy over short-ray paths leading to the seismometer stations from the bottom of the iceberg or near the shore of Ross Island). The strong hydroacoustic coupling implied by this phase interpretation is furthermore consistent with observations of IHT at transoceanic distances, which require strong hydroacoustic coupling of IHT signals to the hydroacoustic waveguide of the ocean (also known as the sound fixing and ranging channel, or SOFAR channel) [*Talandier et al.*, 2002, 2006; *Chapp et al.*, 2005].

[8] The S phase was generally difficult to detect on C16 because the orientation of tremor source slip subevents relative to the stations was nearly optimized for P phase detection (i.e., the stations were located optimally within the $\pm 45^\circ$ radiation lobes emanating from a strike-slip fault created by the edge contact between C16 and B15A, as shown in Figure 3a). However, a second sub-P velocity phase, distinct from the hydroacoustic phase, was detected at station A, which was the station most displaced (by 10°) from the null of the inferred IHT shear wave radiation pattern (stations C and D were displaced by 5° and 3°, respectively; station B was too close to the source to separate the P phase from the sub-P velocity phase). Figure 3d shows the last few distinct subevents immediately prior to the start of the aseismic eye (for 27 December 2003) observed at station A. The seismic displacements for these events are decomposed into radial and tangential components with respect to the source-to-receiver direction. Each subevent produces radial (longitudinal) motions consistent with both P and hydroacoustic arrivals in the frequency ranges and polarizations observed for these phases at other stations (Figures 3a and 3b). The tangential seismic displacement shows the third set (sub-P velocity) of associated arrivals with roughly the same frequency as the P arrival, arriving at an intermediate time between the P and the hydroacoustic arrivals (Figure 3d). The phase speed for this third arrival is between the $\sim$2925 m s^{-1} and the $\sim$1425 m s^{-1} phase speeds of the P and hydroacoustic phases, respectively, and is thus roughly consistent with the $0.53 \times 2925 \approx 1689$ m s^{-1} phase speed expected for S waves in ice [*Kirchner and Bentley*, 1979; *Simmons and Wang*, 1971; *Albert*, 1998], and we interpret this phase as the horizontally polarized S_H phase from IHT subevents predicted by far-field radiation theory from a strike-slip fault of the inferred orientation.

[9] For horizontally propagating seismic waves in thin plates, elastic theory predicts a dispersive transition between 3-D elastic and 2-D "thin plate" theory as wavelength becomes comparable to plate thickness, h, with a reduction in effective bulk modulus occurring with decreasing h [e.g., *Brekhovskikh*, 1960; *Parham and Sutton*, 1971]. Here, because the mean thickness of C16 is estimated to be approximately 100 m, we expect conditions to be near the long-wavelength limit of this behavior because P and S wavelengths are greater than approximately $7h$ (600 and

Figure 3. Iceberg harmonic tremor and its interpretation, shown with seismograms observed on iceberg C16 and Ross Island on 27 December 2003. (a) Vertical channel seismograms for stations B, C, and D filtered to best represent the low-frequency part of the signal (4 pole Butterworth filter between 1 and 3 Hz), and vertical channel seismogram for Ross Island site ABB filtered between 5 and 20 Hz for IHT following the aseismic eye (Figure 2). The horizontal position of each seismogram is plotted as a record section sorted according to great circle distance (at sea level) from the source (Figure 1b). First arrivals of the tremor start phase (yellow dots) on iceberg stations imply a fast phase velocity of $\sim$2925 m s^{-1}, consistent with P waves for a thin Ross Ice Shelf derived iceberg [*Kirchner et al.*, 1979; *Kirchner and Bentley*, 1979]. First arrivals at Ross Island stations show a significantly higher-average propagation velocity of $\sim$4475 m s^{-1}, consistent with horizontally traveling P wave propagation through Ross Island volcanics [*Dibble et al.*, 1994]. (b) As in Figure 3a, except seismograms for the three iceberg stations are filtered to extract the higher-frequency part of the signal. First arrivals of the tremor start phase at stations B, C, and D imply a slow phase velocity of $\sim$1425 m s^{-1}, consistent with $\sim$1450 m s^{-1} hydroacoustic propagation in seawater (1.88 °C and 34.73 psu) below the iceberg and conversion to seismic propagation (for short distance) to reach the receiver at the iceberg surface. Seismograms from ABB (shown) and other Ross Island stations (not shown) display a distinctive increase in tremor envelope amplitude at times consistent with both the large-amplitude waveform associated with tremor restart (Figure 2e) and the $\sim$1450 m s^{-1} hydroacoustic propagation. (c) Highly schematic diagram summarizing phases of propagation. (d) Longitudinal and tangential horizontal (relative to source-receiver direction) ground displacement for station A. Arrival of a horizontally polarized "intermediate" (or S-like) phase is visible in the tangential ground displacement at a time between the P and seismoacoustic arrivals, and is consistent with an expected horizontally propagating S wave phase speed of $\sim$1690 m s^{-1}.

350 m, respectively). Because of the presence of a dissipative and low-velocity firn layer [*Albert*, 1998] of poorly constrained thickness atop C16, the effective elastic thickness of C16 is probably somewhat less than the iceberg thickness, moving this system even further toward the long-wavelength limit. Spectrogram analysis of P and S phases (not shown) confirms this expectation of negligible dispersion in our observed signal frequency range.

2.3. Frequency of IHT Varies With Iceberg Drift Speed

[10] Examination of the drift trajectory of B15A [*MacAyeal et al.*, 2008] during the two IHT episodes illustrated in Figure 2, reveals that the origin of the seismic signals described above lies with the strike-slip motion along a fault that is formed by the edge-on-edge contact between icebergs B15A and C16. Iceberg C16 was motionless throughout the period of observation because it was firmly grounded on the seabed. Iceberg B15A, however, was in a state of constant oscillatory horizontal motion driven by ocean tides [*MacAyeal et al.*, 2008]. The drift of B15A (and the immobility of C16) was observed using navigation-type (single frequency) global positioning system (GPS) receivers (Garmin models GPS36) that were attached to automatic weather stations (AWS) deployed on the icebergs [*MacAyeal et al.*, 2008]. These GPS receivers reported positions on a 20-min schedule with a sensitivity of ±5 m and an accuracy of ±100 m.

[11] The smooth, steady nature of B15A's tidal motion resulting from its large size, was well matched to the accuracy and sample interval of the GPS data. Thus simple, cursory comparisons between the drift trajectory and characteristics of the IHT episode were possible. For the 27 December 2003 IHT episode shown in Figures 2a, 2c, and 2e, six GPS position measurements were obtained during the ~2 h time period during which tremor was recorded. Despite this low sample rate, the iceberg drift trajectory provided strong evidence that properties of the IHT tremor signal were controlled by the relative speed and direction of B15A's motion along the edge contact with C16.

[12] Features notable in the GPS drift trajectory of B15A (Figure 4) are: (1) that B15A's motion was tangential to the B15A-C16 edge contact during IHT generation (Figure 4b), (2) that the rate of iceberg displacement (speed of drift) approximately correlates with the time variation (downward glide) of the fundamental IHT frequency observed in the spectrogram (Figure 4c) and with the time period between tremor subevents (Figures 4d and 4e), (3) that drift ceases during the aseismic eye (Figures 4b and 4c), and (4) that the drift direction reversed and accelerated following the eye, with speed correlating again with the (now upward) glide of the fundamental IHT frequency. Comparison of B15A's drift during the 19 January 2004 event (not shown) and the corresponding IHT spectrogram (Figure 2d) also indicated that tremor frequency correlated with B15A drift velocity. Perhaps the most compelling feature of the iceberg drift trajectory is the fact that the roughly symmetric, concave upward shape of the iceberg drift displacement during the time period IHT shown in Figure 4c matches the chevron pattern of slowly varying frequencies in the IHT spectrograms (Figures 2c and 2d). The number of slip events in the tremor episode of 27 December 2003 is roughly 30,000 (e.g., a 4 Hz subevent rate over a 2 h period of time). The roughly 20 m of displacement during this time period gives roughly 2/3 of a millimeter of slip for each subevent.

[13] The above features are consistent with the origin of IHT being an extended period of stick-slip oscillation generated by the contact between B15A and C16. We propose that movement of B15A during the stick phase of the oscillation allows stress and strain to accumulate in the ice-on-ice contact region. Eventually, the strain exceeds the strength of the ice-on-ice contact, and the system undergoes a rapid slip event, generating an IHT subevent icequake. The time period between subevents is determined by the rate at which stress and strain accumulate in the ice-on-ice contact region, and this rate is determined by the drift of B15A past C16. The characteristic striated, chevron patterns of IHT seen in spectrograms such as shown in Figures 2c and 2d is a consequence of the periodicity of discrete subevents rather than a property of a continuous waveform signifying a "resonant" vibration, such as is a common assumption associated with tremor in other physical systems.

[14] A simple physical analogy for the generation of IHT around the aseismic eye is the children's bicycle noisemaker created by fixing a stiff card in contact with a spoked bicycle wheel. As the wheel spins more slowly, the snapping noise made by the stiff card is less frequent, and the pitch of the perceived sound glides to a lower frequency. When the wheel stops spinning, the noise maker is silent. When the wheel's rotation begins again, but in reverse direction, the snapping noise picks up in frequency, however, the card snaps in the direction opposite to the initial situation.

[15] The chevron spectrogram example for 27 December 2003 does not display as much symmetry as the 19 January 2004 example (Figures 2c and 2d). We attribute this difference to evolving physical conditions such as fault area and contact geometry between the two icebergs during the 27 December 2003 episode. Because this episode was of significantly large amplitude, we ascribe this evolution to edge destructive processes in the source region associated with push mound formation [*MacAyeal et al.*, 2008]. We hypothesize that these edge destructive processes produce the intermittent broadband noise commonly visible on IHT spectrograms (Figures 2c and 2d). For example, as contact geometry changes, the time period between slip events (and consequently, the fundamental tremor frequency) may adjust to maintain constant subevent stress drop conditions. In this model, when the area of contact decreases, the frequency of slip events increases to reflect the correspondingly increased rate of interevent traction accumulation. We also hypothesize that the high-amplitude start-up subevent signifying the resumption of IHT following the aseismic eye (e.g., as shown in Figures 2e and 2f and in Figure 4e) arises because of an ice analogue of fault zone healing [*Li et al.*, 2003], whereby the static shear stress threshold for slip (the static coefficient of friction) is increasing with contact time, perhaps abetted by freezing processes.

2.4. Seismic Radiation Pattern Supports a Strike-Slip Source

[16] First-motion polarities of IHT subevents on either side of the eye (Figures 4d and 4e) are especially illuminating for determining the IHT source process. For IHT observed on 27 December 2003 (Figures 4b and 4c),

B15A's motion was directed South during the preeye tremor (along the same azimuth, approximately 172°, as the edge contact between B15A and C16), and North during the posteye tremor. Horizontal component ground velocity seismograms from station B (Figures 4d and 4e) show sudden, impulsive event onsets with a first motion directed radially (longitudinally) inward toward the inferred source location (as for a dilatational P wave) during the time B15A was moving South. These sudden, impulsive event onsets reversed polarity (were directed radially outward) once the eye of the tremor passed and B15A reversed its drift direction. This polarity change is consistent with P wave seismic radiation generated by elastic rebound stick-slip along a north-striking strike-slip ice-on-ice fault (dip indeterminate, but presumed vertical) in the C16-B15A contact region. This geometry results in right lateral subevent icequakes during the southerly, and left lateral stick-slip events occurring during the northerly drift periods of B15A, respectively.

[17] Additional support for the stick-slip source mechanism operating along the strike-slip edge contact between B15A and C16 is the radiation pattern of P wave, S wave and hydroacoustic wave energy detected by the seismometer array (Figure 4a). The azimuth of the strike-slip edge

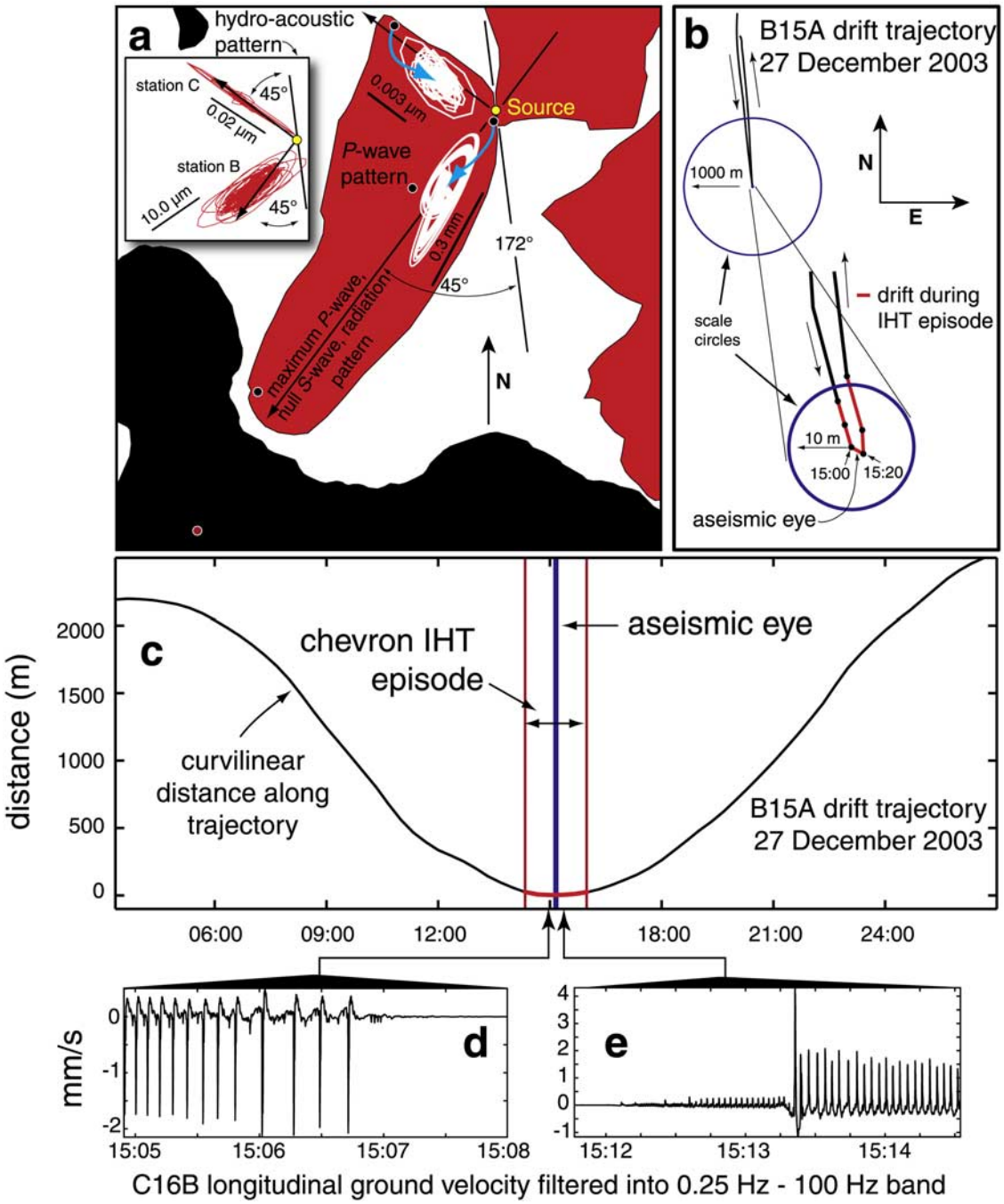

Figure 4

contact between the two icebergs implied by satellite imagery (Figure 1a) is 172°. Stations A, B, C, and D lie at azimuths of 182°, 227°, 312°, and 219°, respectively, relative to the location of the IHT source. The 4 stations are thus arranged at angles ϕ ranging from $\phi = 55°$ for station A to $\phi = 34°$ for station B relative to the trend of the strike-slip edge contact that are close to the ±45° maxima of the $\sin(2\phi)$ radiation pattern associated with P wave energy radiating from a strike-slip fault [*Stein and Wysession*, 2003]. The stations are located in roughly the null radiation zones associated with the $\cos(2\phi)$ S wave radiation pattern from a strike-slip fault. Analysis of P wave seismic displacement at stations B and C is consistent with the expected radiation pattern, because the motions are longitudinally aligned with the source-receiver direction (Figure 4a). The difficulty of detecting S wave arrivals at all stations except A, which was most displaced from the null S wave radiation pattern (station B was too close to the source to facilitate easy differentiation of P and S arrivals), also supports the strike-slip source mechanism along the edge contact fault. Longitudinal alignment with source-receiver direction for the seismic displacements associated with the seismoacoustic phase (again, using frequency band filtering to isolate for station B, and arrival picking for station C) suggests that the hydroacoustic radiation pattern may follow the same $\sin(2\phi)$ pattern associated with P wave radiation from strike-slip faults (inset of Figure 4a).

[18] The observed kinematics of the IHT process clearly indicate that its constituent subevents arise from a stick-slip process. Because 90% of the potential iceberg contact area in the source zone is immersed in the sea, it is also likely that seismogenic slip is taking place in the presence of low-effective stresses resulting from high fluid pressures in the contact zone. Calculations of seismic moments or magnitudes for these subevents are complicated by a present lack of constraint on both the fault dimensions and on the degree of partitioning between aseismic creep and seismogenic slip. It is noteworthy that significant aseismic creep is correlated with the frequency of similar earthquakes arising from asperities on the San Andreas system [*Aster and Scott*, 1993; *Nadeau et al.*, 1995; *Schaff and Waldhauser*, 2005]. For these reasons, we cannot presently offer further quantification of the sources in terms of seismic moment, and a forteriori, cannot yet describe them using the concept of a seismic magnitude. Ongoing work in modeling the Green's function response of slip in this system should ultimately facilitate better constraints on physical size and other source attributes. For the largest IHT events observed to date [*Martin et al.*, 2006], during the grounding-assisted breakup of B15A near Cape Adare, Victoria Land, body wave signals near 1 Hz were observed at distances of up to 18 degrees at the Quiet South Pole seismic station QSPA. This single-station detection is roughly that expected for an earthquake source with energy roughly approaching that of a magnitude 3 earthquake.

3. Conclusion

[19] Our observations show that glancing iceberg collisions at contacts between cliff-like iceberg edges, produce sequences of highly repeatable discrete stick-slip subevents along the ice contact. This regular sequence of pulses forms the IHT signals radiated from Antarctic icebergs. IHT thus belongs to a class of geophysical source phenomena that includes repeating and nonrepeating earthquakes [*Shimazaki and Nakata*, 1980; *Murray and Segall*, 2002], as well as recently described fault zone tremor [*Nadeau and McEvilly*, 2004; *Luan and Robbins*, 2004; *Shelly et al.*, 2006; *Rubenstein et al.*, 2007]. Because of unusually well-constrained conditions, including iceberg masses, forces, geometry, and kinematics, and the relatively high degree of material homogeneity in the ice-ocean system, IHT may be an unusually well-characterized natural laboratory for the dynamic study of large-scale stick-slip systems in physics and in particular geophysics.

[20] Seismic tremor is often (e.g., in the case of volcanic tremor [*McNutt*, 2005]) inferred to arise from an eigenmode of oscillation in a source region that corresponds to a mechanical resonance of the physical system involved. The repeating stick-slip phenomenon described here is not such a resonance, but may be mistaken for such a resonance in far-field seismograms that cannot resolve the individual pulses that make up IHT tremor subevents. In fact, it appears likely that some instances of volcanic tremor are also due to repeating subevents [e.g., *Hellweg*, 2000; *Hagerty et al.*, 2000; *Johnson and Lees*, 2000]. Because of the unusually well constrained kinematics of the iceberg collisions, we can rule out a resonator type source mechanisms for these observations of IHT, Of course, we cannot

Figure 4. Iceberg harmonic tremor source mechanics, P wave and hydroacoustic radiation patterns, and iceberg B15A drift trajectory during the 27 December 2003 chevron-patterned IHT episode (Figure 2c). (a) Map of station geometry and horizontal ground displacements for P waves and seismoacoustic waves (inset) at stations B and C. Alignment of ground displacements with directions ±45° from the trend (~172°) of strike-slip movement of B15A along the collision zone is consistent with the radiation pattern for a strike-slip fault source [*Stein and Wysession*, 2003, p. 221]. (b and c) B15A's drift (measured by single-frequency GPS sampled every 20 min, i.e., 20-min positions of B15A are denoted by dots in Figure 4b) during 27 December 2003. Drift during periods when IHT was observed are indicated by red lines. The flat slope of the red curve in Figure 4c and the reversal of drift direction in Figure 4b indicate that B15A's velocity was zero during the aseismic eye. Changes in IHT fundamental frequency (Figure 2c), dictated by the subevent frequency (Figures 4d and 4e), correlate with drift velocity and the pattern of displacement on either side of the aseismic eye in Figure 4c. (d and e) Longitudinal (source-to-receiver) ground velocity at station B at the beginning and end of the aseismic eye. Impulsive IHT subevent velocity seismogram polarities at seismic stations arise from elastic rebound stick-slip, strike-slip ice-ice faulting in the contact zone driven by B15A's movement (note that subevents reverse seismic polarity as expected across the aseismic eye as B15A drift direction reverses from south to north and the faulting reverses from right to left lateral). It is notable that the first pulse of the restarting IHT (Figure 4e) has larger amplitude than following pulses, suggesting fault strengthening during the repose interval of the aseismic eye.

rule out the possibility that there are other circumstances that might generate tremor-like signals in icebergs (such as hypothesized in the work of *Talandier et al.* [2002], *Chapp et al.* [2005], and Jansen and Müller, submitted manuscript, 2008). In addition to the ice-ice processes noted here, it also appears that the scraping of icebergs along ocean bottom protrusions can produce signals similar to what we have observed in the ice-on-ice episodes discussed here [e.g., *Martin et al.*, 2006].

[21] A principal motivation for the study of glaciogenic seismicity is that it can be used to monitor and quantify some fast timescale processes in ice sheet behavior that are invisible or poorly resolved using geodetic, remote sensing, and other techniques. Recent examples include the acceleration of discharge and calving from marine-terminating outlet glaciers of Greenland [*Ekström et al.*, 2003, 2006; *Tsai and Rice*, 2006; *Tsai and Ekström*, 2007; *Nettles et al.*, 2007] and Alaska [*O'Neel et al.*, 2007], tidally modulated slow seismic events in Antarctic ice streams [*Anandakrishnan et al.*, 2007; *Weins et al.*, 2008] and the calving and subsequent behavior of giant tabular icebergs discussed here. Here, we have determined the source mechanism for a characteristic type of glaciogenic seismicity that may prove relevant to the study of icebergs in a wider context, especially in phenomena where collision and grounding are important [*Swithinbank et al.*, 1977; *Martin et al.*, 2006; *MacAyeal et al.*, 2006]. During the past decade, several large ice shelves in the peninsula region of Antarctica have abruptly disintegrated by breaking up into hundreds to thousands of small icebergs. The unpredictability of the commencement time and short duration of these catastrophic breakup events [e.g., *Rott et al.*, 1996; *Scambos et al.*, 2003, 2005] so far precludes confirmation of driving mechanisms and measures of dynamic processes by conventional means. Teleseismic observation of signals such as IHT generated by disintegrating ice shelves as they convert to collections of mobile, closely packed icebergs may thus provide future insight into this important glaciological process.

[22] **Acknowledgments.** Financial and logistical support was provided by the U.S. National Science Foundation (NSF) under the following grants: OPP-0229546, OPP-0538414, OPP-0229492, OPP-0230028, ANT07-39769, and OPP-0229305. Victor Tsai, Göran Ekström, an anonymous referee, and the associate editor, Gordon Hamilton, contributed substantially to improvements in the manuscript. Various Raytheon Polar Services Co. personnel and crew of the PHI and Kenn Borek aircraft services provided invaluable assistance in seismometer deployments and recoveries. Tim Parker and Noel Barstow of PASSCAL trained the field teams, and Tim Parker participated in the initial field deployment on iceberg C16. Field assistants included Jonathan Thom, Marianne Okal, Andrew Bliss, and various members of the McMurdo Station community. Instruments were provided by the PASSCAL facility of the Incorporated Research Institutions for Seismology (IRIS) through the PASSCAL Instrument Center at New Mexico Tech. IRIS facilities are supported by Cooperative Agreement NSF EAR-000430 and the Department of Energy National Nuclear Security Administration.

References

Albert, D. (1998), Theoretical modeling of seismic noise propagation in firn at the South Pole, Antarctica, *Geophys. Res. Lett.*, *25*(23), 4257–4260.

Anandakrishnan, S., D. A. Wiens, R. B. Alley, R. A. Bindschadler, H. Horgan, L. E. Peters, D. E. Voigt, and J. P. Winberry (2007), Simultaneous GPS and teleseismic monitoring of glacial stick-slip of Whillans Ice Stream, west Antarctica, *EOS Trans. AGU*, *88*(52), Fall Meet. Suppl., Abstract G33C-01.

Aster, R., and J. Scott (1993), Comprehensive identification of similar earthquakes in microearthquake data sets, *Bull. Seismol. Soc. Am.*, *83*(4), 1307–1314.

Aster, R., et al. (2004), Real-time data from Mount Erebus Volcano, Antarctica, *Eos Trans. AGU*, *85*(10), 97, doi:10.1029/2004EO100001.

Brekhovskikh, L. M. (1960), *Waves in Layered Media*, 561 pp., Academic, New York.

Chapp, E., D. R. Bohnenstiehl, and M. Tolstoy (2005), Sound-channel observations of ice-generated tremor in the Indian Ocean, *Geochem. Geophys. Geosyst.*, *6*, Q06003, doi:10.1029/2004GC000889.

Chen, C. T., and F. J. Millero (1977), Speed of sound in seawater at high pressures, *J. Acoust. Soc. Am.*, *62*(5), 1129–1135.

Davey, F. J. (2004), Ross Sea bathymetry, version 1.0, *Inst. Geol. Nucl. Sci. Geophys.* Map 16, scale 1:2,000,000, Inst. of Geol. and Nucl. Sci. Ltd., Lower Hutt, New Zealand.

Dibble, R., B. O'Brien, and C. Rowe (1994), The velocity structure of Mount Erebus, Antarctica and its lava lake, in *Volcanological and Environmental Studies of Mount Erebus, Antarctica*, *Antarct. Res. Ser.*, vol. 66, edited by H. F. Filorn, pp. 1–16, AGU, Washington, D. C.

Ekström, G., M. Nettles, and G. A. Abers (2003), Glacial earthquakes, *Science*, *302*(5645), 622–624, doi:10.1126/science.1088057.

Ekström, G., M. Nettles, and V. C. Tsai (2006), Seasonality and increasing frequency of Greenland glacial earthquakes, *Science*, *311*(5768), 1756–1758, doi:10.1126/science.1122112.

Hagerty, M., S. Schwartz, M. Gearces, and M. Protti (2000), Analysis of seismic and acoustic observations at Arenal Volcano, Costa Rica, 1995–1997, *J. Volcanol. Geotherm. Res.*, *101*(1), 27–65.

Hall, D., G. Riggs, V. Salomonson, N. DiGirolamo, and K. Bayr (2002), MODIS snow-cover products, *Remote Sens. Environ.*, *83*(1–2), 181–194, doi:10.1016/S0034-4257(02)00095-0.

Hellweg, M. (2000), Physical models for the source of Lascar's harmonic tremor, *J. Volcanol. Geotherm. Res.*, *101*(1), 183–198.

Jacobs, S. S., R. G. Fairbanks, and Y. Horibe (1985), Origin and evolution of water masses near the Antarctic continental margin: Evidence from $H_2^{18}O/H_2^{16}O$ ratios in seawater, in *Oceanology of the Antarctic Continental Shelf*, *Antarct. Res. Ser.*, vol. 43, edited by S. S. Jacobs, pp. 59–85, AGU, Washington, D. C.

Johnson, J., and J. Lees (2000), Plugs and chugs—Seismic and acoustic observations of degassing explosions at Karymsky, Russia and Sangay, Ecuador, *J. Volcanol. Geotherm. Res.*, *101*(1), 67–82.

Kirchner, J. F., and C. R. Bentley (1979), Seismic short-refraction studies on the Ross Ice Shelf, Antarctica, *J. Glaciol.*, *24*(90), 313–319.

Kirchner, J. F., C. R. Bentley, and J. D. Robertson (1979), Lateral density differences from seismic measurements at a site on the Ross Ice Shelf, Antarctica, *J. Glaciol.*, *24*(90), 309–312.

Li, Y.-G., J. Vidale, S. Day, D. Oglesby, and E. Cochran (2003), Postseismic fault healing on the rupture zone of the 1999 M7.1 Hector Mine, California, earthquake, *Bull. Seismol. Soc. Am.*, *93*(2), 854–869, doi:10.1785/0120020131.

Luan, B., and M. Robbins (2004), Effects of inertia and elasticity on stick-slip motion, *Phys. Rev. Lett.*, *93*(3), doi:10.1103/PhysRevLett.93.036105.

MacAyeal, D. R., et al. (2006), Transoceanic wave propagation links iceberg calving margins of Antarctica with storms in tropics and Northern Hemisphere, *Geophys. Res. Lett.*, *33*, L17502, doi:10.1029/2006GL027235.

MacAyeal, D. R., M. H. Okal, J. E. Thom, Y.-J. Kim, and A. K. Bliss (2008), Tabular iceberg collisions within the coastal regime, *J. Glaciol.*, *54*(185), 371–386.

Martin, S., et al. (2006), Why do large icebergs fracture at a specific location off Cape Adare?, *EOS Trans. AGU*, *87*(52), Fall Meet. Suppl., Abstract C43B-01.

McNutt, S. (2005), Volcanic seismology, *Annu. Rev. Earth Planet. Sci.*, *32*, 461–491.

Müller, C., V. Schlindwein, A. Eckstaller, and H. Miller (2005), Singing icebergs, *Science*, *310*(5752), 1299.

Murray, J., and P. Segall (2002), Testing time-predictable earthquake recurrence by direct measurement of strain accumulation and release, *Nature*, *419*(6904), 287–291, doi:10.1038/nature00984.

Nadeau, R., and T. McEvilly (2004), Periodic pulsing of characteristic microearthquakes on the San Andreas Fault, *Science*, *303*(5655), 220–222, doi:10.1126/science.1090353.

Nadeau, R. M., W. Foxall, and T. McEvilly (1995), Clustering and periodic recurrence of microearthquakes on the San Andreas Fault at Parkfield, California, *Science*, *267*(5197), 503–507.

Nettles, M., et al. (2007), Short-time-scale variations in flow speed and behavior, Helheim Glacier, East Greenland, *EOS Trans. AGU*, *88*(52), Fall Meet. Suppl., Abstract, C13A-08.

O'Neel, S., H. P. Marshall, D. E. McNamara, and T. W. Pfeffer (2007), Seismic detection and analysis of icequakes at Columbia Glacier, Alaska, *J. Geophys. Res.*, *112*, F03S23, doi:10.1029/2006JF000595.

Parham, R., and D. Sutton (1971), The transition between 2- and 3-dimensional waves in seismic models, *Bull. Seismol. Soc. Am.*, *61*(4), 957–960.

Romero, M. C. R. (2004), Analysis of tremor activity at Mt. Erebus Volcano, Antarctica, M.S. thesis, 159 pp., N. M. Inst. of Min. and Technol., Socorro.

Rott, H., P. Skvarca, and T. Nagler (1996), Rapid collapse of northern Larsen Ice Shelf, Antarctica, *Science*, *271*(5250), 788–792.

Rubenstein, J., J. Vidale, J. Gomberg, P. Bodin, K. Creager, and S. Malone (2007), Non-volcanic tremor driven by large transient shear stresses, *Nature*, *448*(7153), 579–582, doi:10.1038/nature06017.

Scambos, T., C. Hulbe, and M. Fahnestock (2003), Climate-induced ice shelf disintegration in the Antarctic Peninsula, in *Antarctic Peninsula Climate Variability: Historical and Paleoenvironmental Perspectives*, *Antarct. Res. Ser.*, vol. 79, edited by E. Domack et al., pp. 79–92, AGU, Washington, D. C.

Scambos, T., O. Sergienko, A. Sargent, D. MacAyeal, and J. Fastook (2005), ICESat profiles of tabular iceberg margins and iceberg breakup at low latitudes, *Geophys. Res. Lett.*, *32*, L23S09, doi:10.1029/2005GL023802.

Schaff, D., and F. Waldhauser (2005), Waveform cross-correlation-based differential travel time measurements at the northern California seismic network, *Bull. Seismol. Soc. Am.*, *95*(6), 2446–2461.

Shelly, D., G. Beroza, S. Ide, and S. Nakamula (2006), Low-frequency earthquakes in Shikoku, Japan, and their relationship to episodic tremor and slip, *Nature*, *442*(7099), 188–191, doi:10.1038/nature04931.

Shimazaki, K., and T. Nakata (1980), Time-predictable recurrence model for large earthquakes, *Geophys Res. Lett.*, *7*(4), 270–282.

Simmons, G., and H. Wang (1971), *Single Crystal Elastic Constants and Calculated Aggregate Properties: A Handbook*, MIT Press, Cambridge, Mass.

Stein, S., and M. Wysession (2003), *An Introduction to Seismology, Earthquakes, and Earth Structure*, Blackwell, Malden, Mass.

Swithinbank, C. W. M., P. McClain, and P. Little (1977), Drift tracks of Antarctic icebergs, *Polar Rec.*, *18*(116), 495–501.

Talandier, J., O. Hyvernaud, E. A. Okal, and P.-F. Piserchia (2002), Long-range detection of hydroacoustic signals from large icebergs in the Ross Sea, Antarctica, *Earth Planet. Sci. Letts.*, *203*(1), 519–534, doi:10.1016/S0012-821X(02)00867-1.

Talandier, J., O. Hyvernaud, D. Reymond, and E. A. Okal (2006), Hydroacoustic signals generated by parked and drifting icebergs in the Southern Indian and Pacific Oceans, *Geophys. J. Int.*, *165*(3), 817–834, doi:10.1111/j.1365-246X.2006.02911.x.

Tsai, V. C., and G. Ekström (2007), Analysis of glacial earthquakes, *J. Geophys. Res.*, *112*, F03S22, doi:10.1029/2006JF000596.

Tsai, V. C., and J. R. Rice (2006), Possible mechanisms for glacial earthquakes, *Eos Trans. AGU*, *87*(52), Fall Meet. Suppl., Abstract C41A-0290.

Wiens, D. A., S. Anandakrishnan, J. P. Winberry, and M. A. King (2008), Simultaneous teleseismic and geodetic observations of the stick-slip motion of an Antarctic Ice Stream, *Nature*, *453*, 770–774.

R. C. Aster, Geophysical Research Center and Department of Earth and Environmental Science, New Mexico Tech, 801 Leroy Place, Socorro, NM 87801, USA.

J. N. Bassis, Institute for Geophysics and Planetary Physics, Scripps Institution of Oceanography, University of California San Diego, 9500 Gilman Drive, La Jolla, CA 92093, USA.

D. R. MacAyeal, Department of Geophysical Sciences, University of Chicago, 5734 South Ellis Avenue, Chicago, IL 60637, USA. (drm7@midway.uchicago.edu)

E. A. Okal, Department of Geological Sciences, Northwestern University, 1850 Campus Drive, Evanston, IL 60208, USA.